https://doi.org/10.1142/9789811280184_0006

Chapter 6

HL-LHC configuration and operational challenges

Andrea Apollonio, Xavier Buffat, Roderik Bruce, Riccardo De Maria, Massimo Giovannozzi, Giovanni Iadarola, Anton Lechner, Elias Métral, Guido Sterbini, Rogelio Tomás and Markus Zerlauth

CERN,

Esplanade des Particules 1, 1211 Meyrin, Switzerland

Recently, the operational configuration of the HL-LHC along its first Run has been carefully established to reach nominal performance. This chapter presents the key beam and machine parameters together with the most critical operational challenges. The contents of this chapter reflect the project situation prior to experience from the LHC Run 3.

1. Proton parameters and machine optics

The HL–LHC operational scenario for Run 4 is continuously evolving following changes in the hardware configuration, findings in beam dynamics, and schedule updates.[1–3] The latest HL-LHC Interaction Region (IR) layout is shown in Fig. 1 compared to the current LHC. The larger aperture quadrupoles next to the Interaction Point (IP) and the Crab Cavities (CC) allow to reduce the IP beam size while compensating for the loss of geometric overlap during collisions, hence maximizing luminosity. Other key HL-LHC hardware upgrades are described in the following.

The installation of new sextupoles (MS10) in the dispersion suppressor. The loss of Dynamic Aperture (DA, see Sec. 2.3) of about 0.5 σ for not having MS10 is acceptable for optics with $\beta^* \geq 20$ cm in IP1 and IP5, which is the current assumption for Run 4. However, at $\beta^* = 15$ cm, considered for possible new Run 4 scenarios, the DA loss is larger and these sextupoles are mandatory.[4–6] Figure 2 shows the machine optics at $\beta^* = 15$ cm.

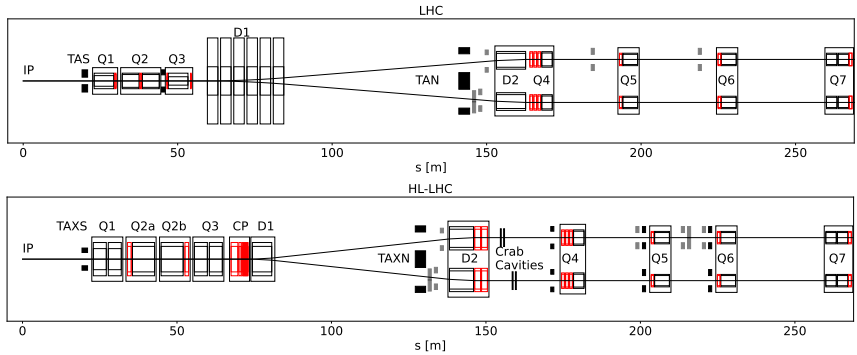

Fig. 1. A schematic comparison of the right side of the interaction region in Points 1 and 5 between LHC (top) and the HL-LHC (bottom). Black boxes represent main magnets and red boxes linear and non-linear correctors. Black filled boxes represent fixed absorbers while gray filled boxes represent collimators. The HL-LHC has large aperture magnets up to D2, a cold D1 and separated D2-Q4 to host the crab cavities.

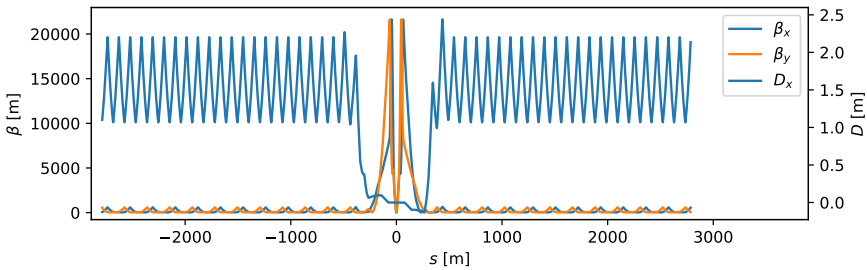

Fig. 2. Plot of the Twiss parameters of the HL-LHC at $\beta^* = 15$ cm. Peak β-function reaches 20 km in the triplet and about 600 m in the arcs around Point 1 and 5. This enhances the sensitivity to field imperfections.

Low impedance upgrade of the secondary Carbon Fiber Composite (CFC) collimators. Most of these collimators are being replaced with Mo-coated collimators, made of Molybdenum-graphite, to guarantee beam stability. Beam experiments in Run 3 should determine if the low impedance collimator upgrade should be carried out in full, whether a reduction in the number of upgraded units would be feasible.

The Hollow Electron Lens (HEL). The HEL is an advanced tool for active control of the diffusion speed of halo particles, which will serve to mitigate losses from fast processes. Due to resource limitations the HEL will not be ready for Run 4. A primary collimator gap at 8.5 σ is considered

the main mitigation against halo issues in the absence of the HEL. The need for additional mitigation measures in Run 4, such as reducing the bunch charge, will need to be evaluated with dedicated measurements in Run 3.

Figure 3 shows a schematic view of the Run 4 operational cycle including key beam parameters and luminosity. The abrupt jumps in bunch intensity and emittances during the collision adjustment process, just before 2.5 h, correspond to the intensity loss and emittance growth budgets assigned for the interval between injection and the start of collisions; however, here they are pessimistically lumped when collisions are established. The slow horizontal emittance growth at injection is due to intra-beam scattering

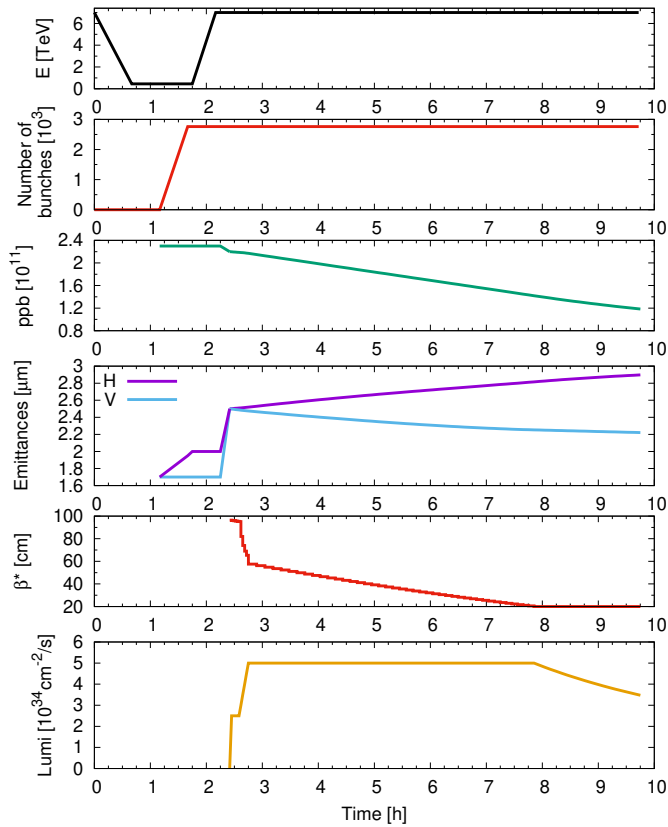

Fig. 3. A schematic view of the Run 4 HL–LHC physics cycle showing energy cycle, number of bunches, protons per bunch (ppb), transverse emittances (Batch Compression Merging and Splitting beam case), and luminosity (top to bottom) versus time until the beam dump.

(IBS). The luminosity starts with a step at 2.5×10^{34} cm^{-2}s^{-1} followed by a linear ramp to meet cryogenic requests. The bunch intensity and emittance evolution during physics include burn-off, IBS, synchrotron radiation (SR) damping, and emittance growth from CC noise. Emittance growth from luminosity burn-off has a small effect on the integrated luminosity of HL–LHC of approximately 1%, not included here, and should be further studied for more accurate predictions.[7]

Assuming no limitations to the beam parameters in Run 4, the potential HL–LHC performance ramp-up is given in Fig. 4, allowing to integrate above 715 fb^{-1} over the 4 years of operation. The minimum β^* in Run 4 is tentatively kept to 20 cm but 15 cm is being considered.

In the first year of operation, bunch intensity is assumed to match the updated Run 3 expectation of 1.8×10^{11} ppb with minimum $\beta^* = 30$ cm and without CCs in physics (but commissioning them with dedicated machine time). Crossing angle is assumed to be about 450 μrad as validated with DA simulations. It is foreseen to steadily reduce the crossing angle during the physics fill as the bunch population decays to maximize performance and reduce the peak radiation dose to the triplet magnets.

The beam-based IR non-linear corrections are expected to require considerable commissioning time and iterations between the different magnet types. Therefore, it is assumed that optics commissioning in the first years will only include correction magnets up to the octupolar order, leaving the commissioning of the decapolar and dodecapolar correctors for the years with lower β^*. Simulations have confirmed that DA is sufficient at $\beta^* = 30$ cm without decapolar and dodecapolar IR corrections. Moreover,

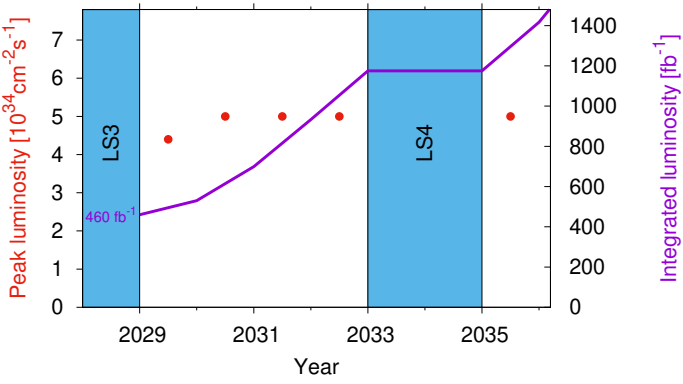

Fig. 4. Peak and integrated luminosity during Run 4.

techniques to speed-up the optics commissioning including high-order corrections are being developed and will require dedicated machine experiments in Run 3.

Bunch intensity could be limited in Run 4 due to the absence of the HEL or if RF voltage limitations are encountered at injection. Taking these aspects into account, a minimum bunch intensity of 1.8×10^{11} ppb is estimated to be easily achievable. Further studies are ongoing to investigate the maximum bunch intensity feasible with the current RF system. If bunch charge is limited to 1.8×10^{11} ppb at injection, the fill shortens by more than 2 hours and the levelling time by more than 3 hours with respect to the baseline shown in Fig. 3. Annual integrated luminosity (assuming 160 days) is reduced from 242 to 194 fb^{-1}, reducing the Run 4 expected integrated luminosity by about 20% for the case with $\epsilon = 2.5$ μm. Figure 5 shows the annual integrated luminosity versus bunch charge at injection in the range between 1.8×10^{11} ppb and the baseline value. Mitigation measures imply reducing β^* or the crossing angle. The first requires that the MS10 sextupoles are installed during Long Shutdown 3 (LS) to guarantee sufficient lifetime. The latter requires that long-range beam-beam compensators, not yet in the baseline, are installed.

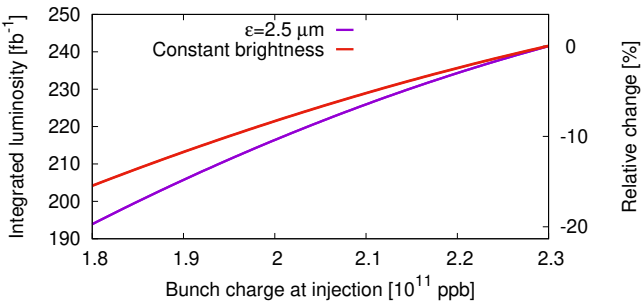

Fig. 5. Annual integrated luminosity versus bunch charge at injection in Run 4.

In the following the most critical operational challenges are reviewed.

2. Proton operational challenges

2.1. *Heat load and e-cloud*

The LHC and HL-LHC cryogenic magnets are equipped with actively cooled beam screens, which intercept beam induced heating mainly due to

synchrotron radiation, impedance and e-cloud effects. During the LHC Run 2 large heat loads were observed on the beam screens during operation with the nominal bunch spacing of 25 ns. In particular, the heat loads in some of the arcs reached levels close to the design cooling capacity of 8 kW/arc. In all sectors, the heat-loads were significantly larger than expected from impedance and synchrotron radiation.[8–10]

By analyzing the heat load data collected during Run 2 and comparing them against models and simulations, it was possible to conclude that a dominant fraction of the observed heat loads is due to electron cloud effects, as a result of a larger than expected Secondary Electron Yield (SEY) of the beam screen surfaces. During the LS2 (2019–2022) surface analyses were conducted of beam screens extracted from the accelerator, which identified specific surface modifications associated with the magnets showing the highest heat load, namely the presence of cupric oxide (CuO) and a very low carbon concentration. These modifications are associated with a larger SEY and therefore with a stronger e-cloud.[11]

Numerical simulations can be used to estimate the arc heat loads expected for the HL-LHC beam parameters. Figure 6 shows the arc heat loads expected for the most critical LHC arc (S81) as a function of the bunch intensity. The predictions are made assuming for each cryogenic cell the SEY estimated from heat load measurements collected during Run 2. It can be observed that the heat load contributions from e-cloud are not expected to increase significantly for intensities above 1.8×10^{11} p/bunch. Such a feature has been confirmed experimentally using short bunch trains at the end of Run 2.[12]

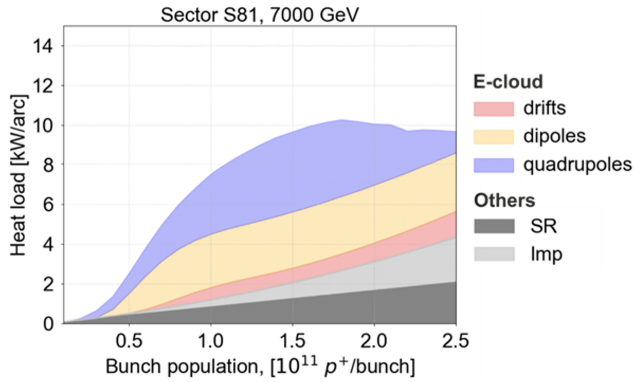

Fig. 6. Expected heat loads at 7 TeV as a function of the bunch intensity for the most critical arc of the LHC (to be compared to the available cooling capacity of 10 kW/arc).

During Run 2, the LHC cryogenics has been operated in an optimized configuration (using one cold-compressor unit to serve two consecutive sectors). The cryoplants feeding the high-load sectors have been recently characterized by the cryogenics team, and they were found to perform better than their design specifications, being able to deliver 10 kW/arc. Assuming that the cryoplants can reliably provide such a cooling capacity and that no degradation of the SEY will take place after Run 2, the HL-LHC nominal beam configuration is expected to be compatible with the limits defined by the cryogenic system. In case these conditions are not met, surface treatments will need to be performed in order to reduce the SEY of the beam-screen surfaces. Alternatively, hybrid filling patterns could be used to partially mitigate the performance loss.[13]

2.2. *Beam instabilities*

Once the machine is well scrubbed, the main limitation due to beam instabilities occurs at flat top, mostly because of the impedance of the collimators. Indeed, to maintain the cleaning efficiency, the collimators move closer to the beam during the energy ramp, following the adiabatic damping of the transverse emittances. This significantly increases their impedance. At the same time the reduction of the physical emittance of the beam reduces the effectiveness of the Landau octupoles. These magnets located in the arcs generate a spread in the transverse tunes, thus stabilising the so-called weak head-tail instability driven by the machine impedance via the mechanism of Landau damping. The strength of the damping is however limited by the maximum strength of the octupole magnets and by their detrimental impact on the beam lifetime.[14] In order to allow for the highest beam brightness without exceeding those limits, new collimators were designed with the goal of maintaining the robustness to radiation, while reducing their resistivity and consequently their impedance. While the LHC collimators are based on CFC jaws, the new primary and secondary collimators are based on Molybdenum-Graphite blocks. The secondary collimators feature in addition a Molybdenum coating[15] in order to optimise their impedance. Along with this technological improvement, it is necessary to master the various mechanisms that affect Landau damping taking into account the operational constraints.

Non-linear magnetic components in the final focusing quadrupoles can significantly impact the tune spread when the beams are squeezed at the IP. Since this contribution may enhance or cancel the tune spread driven

by the Landau octupoles in an uncontrolled manner, the measurement and correction of these non-linearities is critical to maintain the beam stability.[16] Linear coupling can severely reduce the tune spread driven by the octupoles.[17] This mechanism caused several instabilities leading to beam aborts during the first run of the LHC. With the implementation of an online coupling measurement and correction tool, this instability was no longer observed. A tight control of linear coupling will be needed for the HL–LHC.[14]

The beam-beam interactions also affect the beam stability, mainly through their impact on the tune spread.[14] The polarity of the octupoles is chosen to interact constructively with the long-range beam-beam interactions which dominate in the phase from the end of the ramp to the start of collision. This phase is indeed the most critical for beam stability, since afterwards the head-on collisions generate a much larger tune spread which efficiently suppresses all expected instabilities. Configurations featuring an offset between the beams in the order of the transverse rms beam size require a special attention due to the very specific non-linear behaviour of the beam-beam force in this range. Yet no performance limitations are expected due to this effect in the HL–LHC.

The relation between instabilities arising with a latency of several minutes and noise acting on the beam was both observed and explained.[18] This mechanism of loss of Landau damping puts tight constraints on the noise of existing and new equipment. In addition, this mechanism favours shortening of the most critical phase, i.e. between the end of the ramp and the establishment of collisional orbits. The operation with a combined ramp and squeeze as well as β^* levelling is therefore greatly beneficial, by reducing to the minimum the phase of the β^* squeeze with non-colliding beams.

2.3. *Beam lifetime*

The expected performance of the HL–LHC relies not only on very challenging beam parameters, e.g. beam intensity and emittance, to be achieved at the start of the luminosity production, but also on preserving those parameters throughout the luminosity production period of the fill. The beam lifetime is the figure of merit to quantify the time constant of the beam intensity decay. In an ideal collider, the beam lifetime should be dominated by the burn-off losses induced by luminosity.

The approach assumed at the time of the LHC design[19] evolved quite

strongly after the beginning of the operations. Indeed, the original paradigm based on well-separated, quasi-static, and sequential changes to the ring optics has been replaced, following also the implementation of the so-called Achromatic Telescopic Squeeze (ATS) optics,[20] by rapid and parallel changes to the machine configuration, encompassing, as an example, squeeze of the insertion optics and variation of the strength of the Landau octupoles to fight collective instabilities. A similar approach has been extended to the stage when the beams are put in collision, when several luminosity levelling options have been already implemented, such as levelling by varying the parallel separation and the crossing angle of the beams at the interaction points.

This dynamic environment is applied to a system in which nonlinear effects perturb the beam motion, be them generated by the unavoidable magnetic field errors stemming from the superconducting magnets or the strong beam-beam interactions. Nonlinear effects induce resonance excitation, which, combined with IBS, synchrotron radiation, luminosity effect,[21,22] and with other time-dependent perturbations, lead to emittance growth or degradation of the beam lifetime, finally affecting the collider performance in terms of luminosity evolution.

Possible sources of time-dependent perturbations are the ripples in the power converters of the various magnet families, perturbations coming from the UPS connected to the machine electronics, or from specific devices, e.g. CC,[23] transverse damper,[24] HEL,[25,26] etc. In the HL–LHC, the revolution frequency is about 11.24 kHz, and a noise spectrum with frequency larger than about 1 kHz can affect the beam lifetime. As an example, the power converter ripples may introduce pseudo-random effects in the beam dynamics, thus creating a diffusive behaviour of the beam distribution leading to emittance growth and losses that affect the beam lifetime. For these reasons, important efforts are devoted to scrutinize the limiting circuits of the machine[27–29] with the goal of devising mitigation measures to the ripples on existing and new power converters. As an example, in Fig. 7 we report, starting from the measured LHC transverse noise spectra of the beams, the simulated impact on Beam 1 (B1 - the clock-wise beam) and Beam 2 (B2 - the counter-clock-wise beam) intensity decay. The simulations are in agreement with the observed lifetime difference of the two beams in LHC.

In this light, the design studies for the HL–LHC have tackled a series of new challenges. Since the LHC design, the concept of DA, i.e. the extent of the phase-space region in which bounded motion occurs, has been used as the key figure of merit to scrutinize the suitability of the field quality

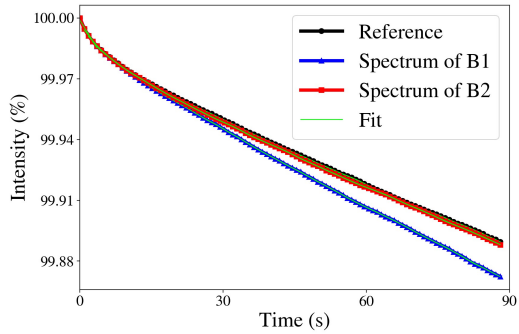

Fig. 7. Intensity evolution in the absence of power supply ripple (black), including the measured power supply ripple spectrum of Beam 1 (blue) and Beam 2 (red) (the parameters used for the numerical simulations are listed in Ref. 28).

of the various magnet families.[19,30] To make such a rather abstract, i.e. not directly observable using the machine diagnostic, figure of merit better suited to the analysis of the actual collider performance, a link between DA and beam lifetime has been established[31] and used also to derive models for the luminosity lifetime.[32,33] Experimental methods to determine the DA in a circular accelerator[34] were developed (note that a qualitative DA estimate was obtained by displacing the beam close to the DA border,[35]) together with improved tracking capability leveraging on the potential of the Graphical Processing Unit hardware.[36,37]

It is worth noting that a consistent approach to the determination of the beam lifetime has to be complemented by means and tools to determine the evolution of the beam distribution, which is of paramount importance to assess emittance growth and beam losses. Therefore, new emphasis has been put on the long-term numerical tracking (e.g. about 30 min, corresponding to 2×10^7 turns in the LHC) and the derivation of diffusive models, basing this framework on a fundamental theorem of the theory of dynamical systems, i.e. Nekhoroshev theorem.[38–40] This led to a number of successful analyses of beam measurement taken at top energy in the LHC[41,42] and to a possible revision[43] of the so-called collimator scans that are used to determine the diffusion coefficient for the LHC beam dynamics.[44,45] This research is currently in full development and future steps include the development of diffusive models for systems with two degrees of freedom and the possibility of extracting information on the diffusion coefficient from dedicated tracking simulations. Accurate information on the evolution of

the beam distribution over realistic time scales would then be obtained by solving the Fokker-Planck equation with the diffusion coefficient determined by direct tracking. This approach would have also the advantage that solving Fokker-Plank equations over a time scale compatible with the actual machine cycle is certainly more affordable, in terms of CPU power required, than carrying out element-by-element tracking simulations over the same time scale.

2.4. *Machine availability*

Large-scale research infrastructures and in particular circular colliders such as the LHC represent a major challenge in terms of equipment reliability, as many ten thousand accelerator and infrastructure components must operate simultaneously and continuously for many hours to produce the desired physics output. For HL-LHC, the nominal fill length (including the leveling period) will be in the order of 7.5 hours, which will be interleaved with a turn-around time of at least 2.5 hours to bring back the beams into collisions after a machine failure or a deliberate termination of the prior physics fill. Therefore, in addition to the accurate and reliable control of proton and ion beams, with twice and five times the stored beam energy of the nominal LHC design respectively, machine operation in the HL-LHC era will also require further improvements of the already outstanding machine availability that was steadily improved during the first two operational runs.[46] During the three final years of its second operational run, the LHC managed to produce particle collisions during almost half the time devoted to high-intensity proton operation, while the remaining time was equally shared between equipment failures and regular operational time (such as the injection of beams from the injectors or the energy ramps). This is an unprecedented achievement for such a complex machine, which in addition is using many novel technologies that were never used at such industrial scales before. One of the main reasons for this achievement is that dependability considerations were a fundamental part of every equipment design from the very beginning. This is in particular the case for the backbone of the machine protection system, for which state of the art reliability engineering methods were employed to guarantee meeting both, the challenging reliability as well as availability targets. The second, equally important ingredient is a continuous identification and documentation of the root causes of down-time arising during the operational periods of the accelerator equipment. A dedicated tool, the so-called Accelerator Fault Tracker (AFT)

has been developed to this end, allowing to identify and quantify the impact of recurring equipment failures on machine operation and trigger targeted consolidation activities to mitigate these weaknesses. Examples are major consolidation or displacement activities for electronics installed close to the accelerator which have shown weaknesses to radiation induced effects, the optimization of interlock levels across numerous protection systems based on beam operation experience and the preventive replacement of several thousands of local power supplies with unsatisfactory reliability. Another important ingredient is the development of more and more powerful operational tools, both for the diagnostic of the machine state as well as for the automation of recurrent operations and adjustments, which ensure repeatability while avoiding as much as possible human errors in the execution of the complex operational sequences. Following these continued efforts, LHC availability has today reached a level where it is dominated on one hand by the availability of its injector complex, and on the other hand by a few, but often long stops in the infrastructure systems necessary for the operation of the large superconducting magnet system as shown in Fig. 8. The full injector complex underwent a major upgrade program during the second long shutdown (LS2),[47] the impact of which on overall availability will only become visible during the upcoming Run 3. Failures in particular in the cryogenic system on the other hand will, despite often minor root causes, require many hours to recover nominal operating conditions as employing redundancy techniques is only possible to a very limited extent in such large-scale industrial systems.

As the complexity of the LHC will further increase with the deployment of the HL-LHC upgrade, it is therefore important to maintain and even further improve the availability for HL-LHC operation as shown in Fig. 9. This is not only true for the newly installed machine components, but also for the remaining parts of the machine which are based on components that will approach the end-of-life at the time of the HL-LHC era. Pursuing preventive maintenance and consolidation activities as well as further improvements of intervention procedures are therefore a necessity, limiting as much as possible the need of physical access to the tunnel to perform corrective actions.

2.5. *Energy choice and beam-induced magnet quenches*

The LHC has been designed for a center of mass collision energy of 14 TeV, and all superconducting main dipole magnets have been individually

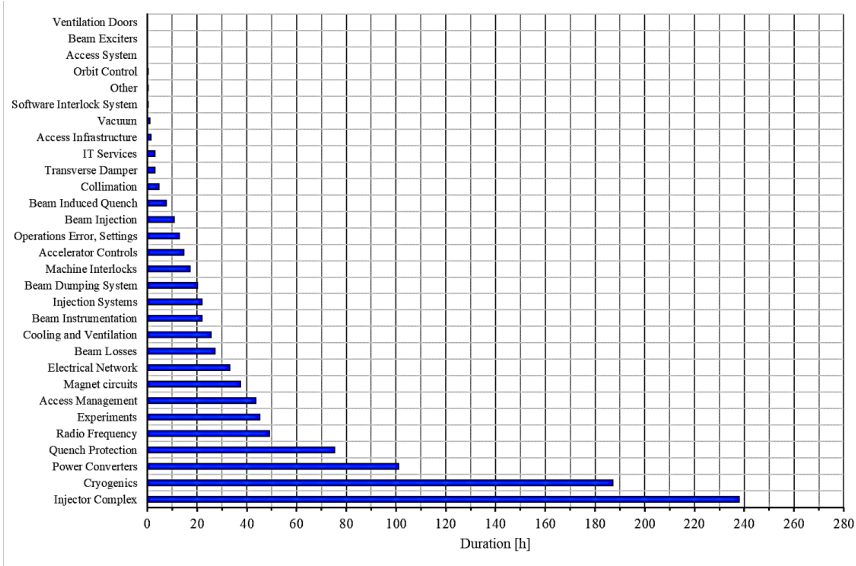

Fig. 8. Downtime of the LHC as a function of the root cause failure during the last year of Run 2 in 2018.

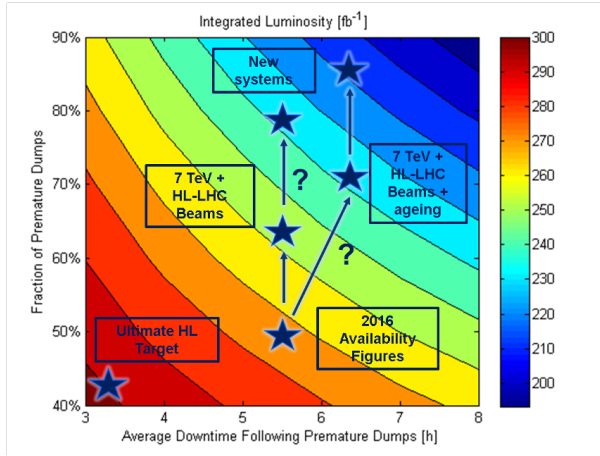

Fig. 9. Yearly luminosity reach of the LHC as a function of premature beam dumps and the average downtime caused. The availability figures reached during a typical Run 2 year (2016) are highlighted along with the HL-LHC target and possible negative performance impacts.

qualified beyond their nominal energy of 7 TeV before their installation in the LHC tunnel. Recent experience after thermal cycles of the machine (which are required to allow for the extended maintenance periods at the end of a typically 3–4 yearlong operational run) show that most main dipole magnets will require a (re-)training quench to reach their nominal current again (see Fig. 10). Combined with secondary quenches due to electromagnetic and thermal coupling this results in an unexpectedly large number of (re-)training quenches that are necessary to restore the operating energy.

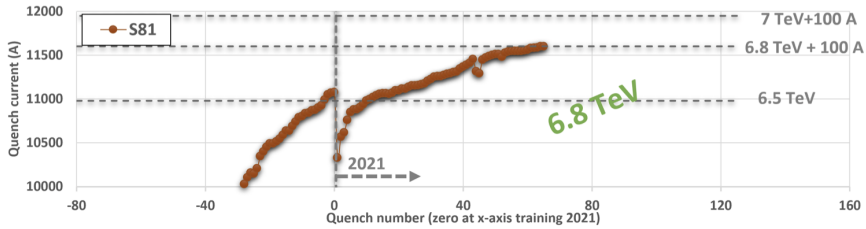

Fig. 10. Circuit current as a function of number of (re-)training quenches in LHC sector 81. During Run 2, the machine was operated at 6.5 TeV, while the 2021 commissioning campaign pushed the sector to achieve the 6.8 TeV energy equivalent.

In addition to the considerable amount of time that needs to be spent for the magnet training, repeated quenches of magnets also represent a certain risk for the mechanical and electrical integrity of the superconducting elements, potentially requiring the repetition of a thermal cycle if major non-conformities arise during the training campaign. For these reasons, the operational energy for LHC Run 3 has been limited to 6.8 TeV, further postponing the commissioning of the entire LHC to nominal energy until a future operational run. Experience has however shown that operation at lower beam energies, while decreasing peak luminosity, can be beneficial for the overall physics output of the machine as the loss in peak performance is largely compensated by the gain in machine availability when operating with increased margins. This is true for many accelerator systems such as power converters, cryogenic equipment, etc., but also for their interplay with the high intensity particle beams, such as the increased likelihood of beam induced quenches of superconducting magnets when operating at higher beam energies. Controlling the losses of highly energetic particles in a superconducting accelerator is a challenging task, especially for localized loss events which can be caused by fast beam instabilities or interactions of the proton beams with dust particles (UFOs). The latter were the main

reason for beam-induced quenches in Run 2,[48] and they are expected to remain the primary source of transient beam loss events in future runs. When entering the beam, dust particles get rapidly ionized and are repelled from the circulating protons within a few turns of the beams. While most events are harmless, a small fraction of dust particles can still induce sufficient beam losses to perturb beam operation. This fraction will, however, increase in future runs due to more challenging operational conditions.

An efficient protection of the magnets against beam-induced quenches requires an in-depth understanding of the underlying physics of the energy deposition mechanisms as well as the quench limits of the different superconducting magnets. Both have been extensively simulated and empirically studied during the first two operational runs of the LHC, allowing a good compromise between beam loss protection settings and beam-induced magnet quenches to be defined. Figure 11 shows the maximum energy density in dipole coils for different dust events observed at 6.5 TeV in Run 2 (left plot). The energy density values were obtained by means of particle shower simulations. Events, which resulted in a quench, are displayed as crosses, whereas events without quench are represented by dots. As illustrated in the right plot, the number of quenches in Run 2 would have been higher, had the operational energy been 6.8 TeV as in Run 3. The energy increase reduces the quench limit of the main dipole magnets by 20%, while the same number of lost protons will lead to 7–8% higher energy densities in the magnet coils. This increased likelihood of beam induced quenches and in general reduced operational margins will very likely require further optimizations of the protection thresholds and strategies as a function of the

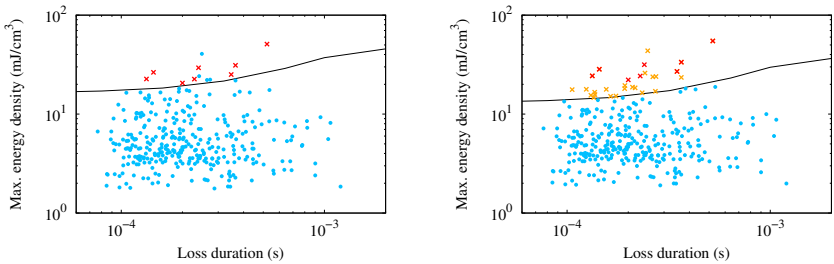

Fig. 11. Maximum energy density in dipole coils for different dust-induced loss events. Events without quench are shown as blue dots, whereas events with quench are shown as crosses. The solid line represents the quench level. The left figure illustrates the actual situation in Run 2 (6.5 TeV), while the right plot shows the expected number of quenches if the beam energy would have been 6.8 TeV.

experience gained when operating at increased beam energies approaching the nominal energy of 7 TeV.

3. Ion operation and challenges

Apart from the main physics programme with proton collisions, the LHC has also been designed to collide heavy ions. So far, the LHC has typically operated for about one month per year with heavy-ion beams, mainly fully stripped Pb nuclei. Initially, the goal was mainly to provide Pb-Pb collisions to ALICE, which is specialised in heavy-ion physics, but over time all the LHC experiments have joined the heavy-ion programme.

Operation with Pb ions entails different challenges and limitations from proton operation. The magnetic fields are the same, however, since the charge-to-mass ratio is lower, the energy per mass is also lower (2.76 TeV per nucleon for Pb and 7 TeV per proton in the LHC design scenario). The Pb ion bunch charge is only about 15% of the proton bunch charge, however, each $^{208}Pb^{82+}$ ion has 82 times higher charge and about 208 times higher mass than a proton. Because of this, limitations from beam-beam effects and machine impedances are more relaxed, although IBS and radiation damping are stronger. Furthermore, the total interaction cross section is more than 6000 times larger for Pb ions than for protons. This results in a much larger fraction of ions colliding at every passage through the collision point, and hence a very rapid burn-off of the beam.

It should also be noted that the interaction cross section is strongly dominated by ultraperipheral electromagnetic interactions, which occur in about 98.5% of all collision events. These interactions take place when two colliding ions pass close to each other without a direct nuclear overlap, as opposed to the hadronic nuclear interactions where the nuclei physically overlaps. The hadronic nuclear interactions, occurring only in about 1.5% of the events, are usually the main object of study of the experiments.

So far four one-month runs have been carried out with Pb-Pb,[49–51] and two runs with proton-Pb collisions. So far, the integrated luminosity for Pb-Pb collisions (corresponding to the total amount of data collected by the experiments) is $2.5\,\mathrm{nb}^{-1}$ at ATLAS and CMS, $1.5\,\mathrm{nb}^{-1}$ at ALICE and $0.25\,\mathrm{nb}^{-1}$ at LHCb. It should be noted that an integrated luminosity of $1\,\mathrm{nb}^{-1}$ corresponds to about 5.15×10^{11} collision events for Pb-Pb. For p-Pb collisions, an integrated luminosity of about $250\,\mathrm{nb}^{-1}$ has been collected at ATLAS and CMS, $75\,\mathrm{nb}^{-1}$ at ALICE and $36\,\mathrm{nb}^{-1}$ at LHCb, where $100\,\mathrm{nb}^{-1}$ corresponds to 2.2×10^{11} p-Pb collision events.

It has been planned for the LHC heavy-ion programme to continue in the future LHC and HL-LHC operation in Run 3 and Run 4, still using Pb-Pb and p-Pb collisions. The target for the ALICE physics programme after the proposed upgrade have been set to $13\,\mathrm{nb}^{-1}$ of integrated Pb–Pb luminosity during the next eight years of operation,[52,53] which requires producing almost nine times more collision events than what has been produced so far in the first eight years (in about the same amount of time). A similar increase in p-Pb collision events is also required.

A detailed machine scenario for future heavy-ion operation has already been devised,[54,55] containing the configuration of all relevant accelerator subsystems. Numerical simulation models of the ion beam evolution, including a range of physical effects, are used to study the development of the luminosity, intensity, and emittance.[55] These studies show that the physics goals are just within reach, however, there is a significant error bar on the input conditions, such as the achievable intensity and the machine availability. Therefore, various performance improvements are being studied, such as decreased beam size at the collision points, or smaller crossing angles, which would boost the luminosity.[55]

Dedicated upgrades of the LHC and the injectors are necessary in order to reach these ambitious goals. Firstly, a new method of stacking the bunches in the Pb beam more closely together will be implemented in the SPS. This method, called slip-stacking,[47] relies on an upgrade of the RF system in the SPS and allows shortening of the spacing between the bunches from 75 ns to 50 ns. Hence about 70% more bunches can be fitted in the LHC, following also optimizations in the pattern of injected bunches into the LHC. This allows significant increasing of the luminosity, most notably by more than a factor 6 at ALICE.[55] A first demonstration of the slip-stacking in the SPS was done in 2021.

The higher beam intensity and luminosity entail significant operational challenges connected to beam losses, where the most serious one is connected to the ultraperipheral electromagnetic interactions. The most common one is called bound-free pair production (BFPP). It causes the creation of an electron-positron pair, where the electron is caught in a bound state at one of the colliding nuclei, hence changing its charge. Therefore, the magnetic force on the affected ions is reduced, so they follow a dispersive trajectory and eventually impact on the machine aperture a few hundred metres downstream of the collision point.[56,57] Such beam losses due to BFPP have been observed both at RHIC[58] and at the LHC.[59]

Losses from BFPP, carrying a total power of up to about 165 W at

HL-LHC, would heat the impacted magnet such that it loses its superconducting state (a so-called quench). Quenches must be avoided by all means during collider operation as the recovery is a lengthy process that reduces the available time for physics operation. Therefore, these losses will be mitigated by redirecting them with a local orbit bump into a safe location: either an empty connection cryostat, or newly installed collimators. This alleviates the risk of quenches at the luminosities considered for Run 3 and HL-LHC.[59]

Electromagnetic dissociation is another ultraperipheral interaction, where one nucleus emits one or several nucleons, hence changing the charge-to-mass ratio and the trajectory of the affected ions. These processes are, however, less hindering for operation, since they either carry only a small amount of power and can be intercepted by collimators.

Another serious operational challenge comes from the higher beam intensity, and hence higher stored beam energy. It will exceed 20 MJ for Pb beams, which makes the LHC beams highly destructive, since even minor beam losses could cause magnet quenches or even damage. Therefore, beam losses need to be tightly controlled and safely intercepted by a collimation system, consisting of several stages of massive absorbers.[60–64] The same collimation system was used during Run 1 and Run 2 for protons and heavy ions, but the cleaning process is about two orders of magnitude less efficient for ions, due to nuclear fragmentation processes inside the primary collimators. Affected ions, with altered charge-to-mass ratio, can exit the collimator material and continue through the beam pipe on dispersive trajectories until they are lost.[65,66] Therefore, the collimation performance is more critical for heavy ions than for protons, in spite of lower stored beam energy, and the inefficiency of the present collimation system risks limiting the machine availability due to frequent beam aborts.

To overcome this limitation, the future collimation system for heavy ions is based on a fundamentally different principle, called crystal channeling. A silicon crystal, only a few millimeters long and bent with curvature of about 50 μ rad, replaces the role of the present massive primary collimators.[67,68] Inside the crystal, any intercepted ions are captured in a potential well between the crystalline planes, a "channel", where it can propagate with a strongly reduced probability of interacting with the atoms of the crystal. The bending of the channel causes affected ions to exit the crystal with an angular kick, strong enough to make it hit so deeply inside the standard secondary collimators (that are used as absorbers), that the risk of any secondary ion fragments leaking out is greatly reduced. With this

technique, the efficiency of the collimation system can be improved sufficiently to safely store the future Pb beams. Following successful tests in previous LHC runs, new crystal collimators have been installed in the LHC for operational deployment in Run 3.[69]

The present heavy-ion physics programme, based on Pb beams, is scheduled to continue until the end of Run 4. Starting from Run 5, a new programme is proposed and under study,[53] which relies on upgraded experimental detectors that can digest a much higher luminosity. In order to provide this luminosity, the possibility of operating the LHC with ion species other than Pb is being investigated. Such beams have the potential of a significantly increased intensity and nucleon-nucleon luminosity, however, limitations in the injector complex as well as in the LHC require further studies.

References

1. G. Arduini et al., HL–LHC Run 4 proton operational scenario. Technical Report CERN-ACC-2022-0001, CERN (2022).
2. E. Métral et al., Update of the HL–LHC operational scenarios for proton operation. Technical Report CERN-ACC-NOTE-2018-0002, CERN (January, 2018). URL `https://cds.cern.ch/record/2301292/files/CERN-ACC-NOTE-2018-0002.pdf`.
3. R. Tomás et al., Operational scenario for the first HL–LHC run. In *Proc. 13th Int. Particle Accelerator Conf. (IPAC'22)*, JACoW Publishing (2022).
4. S. Kostoglou and R. De Maria, Reviewing the "No MS10" scenario during collisions for Run 4 with DA beam-beam simulations (2021). 132$^{\text{nd}}$ HL-LHC TCC meeting, `https://edms.cern.ch/document/2569782/1`.
5. R. De Maria and S. Kostoglou, Review of the situation without MS10 at the beginning of collisions and at the end of leveling (2021). 189$^{\text{th}}$ HL-LHC WP2 meeting, `https://indico.cern.ch/event/1014471/`.
6. S. Kostoglou, H. Bartosik, R. D. Maria, Y. Papaphilippou, G. Sterbini, and R. Tomás, Dynamic aperture studies for the Run 4 High-Luminosity LHC operational scenario, in preparation.
7. R. Tomás, J. Keintzel, and S. Papadopoulou, Emittance growth from luminosity burn-off in future hadron colliders, *Phys. Rev. Accel. Beams.* **23**, 031002 (Mar, 2020). doi: https://doi.org/10.1103/PhysRevAccelBeams.23.031002. URL `https://journals.aps.org/prab/abstract/10.1103/PhysRevAccelBeams.23.031002`.
8. G. Iadarola, B. Bradu, P. Dijkstal, L. Mether, A. Romano, G. Rumolo, G. Skripka, and L. Tavian, Electron Cloud and Heat Loads in Run 2. In *9th LHC Operations Evian Workshop*, pp. 221–232, Geneva, Switzerland (2019).
9. G. Skripka, P. Dijkstal, G. Iadarola, L. Mether, G. Rumolo, and E. G. T. Wulff, Comparison of electron cloud build-up simulations

against heat load measurements for the LHC arcs with different beam configurations. In *Proc. 10th Int. Particle Accelerator Conf. (IPAC'19)*, pp. 3232–3235, JACoW Publishing (May, 2019). doi: doi:10.18429/JACoW-IPAC2019-WEPTS051. URL http://accelconf.web.cern.ch/ipac2019/papers/WEPTS051.pdf. https://doi.org/10.18429/JACoW-IPAC2019-WEPTS051.

10. G. Iadarola et al., Progress in mastering electron clouds at the large hadron collider. In *Proc. 12th Int. Particle Accelerator Conf. (IPAC'21)*, pp. 1273–1278, JACoW Publishing (May, 2021). doi: doi:10.18429/JACoW-IPAC2021-TUXA03. URL https://jacow.org/ipac2021/papers/TUXA03.pdf. https://doi.org/10.18429/JACoW-IPAC2021-TUXA03.
11. V. Petit, M. Taborelli, D. A. Zanin, M. Himmerlich, H. Neupert, P. Chiggiato, and G. Iadarola, Beam-induced surface modifications as a critical source of heat loads in the Large Hadron Collider, *Communications Physics*. **4** (1), 1–10 (2021). ISSN 23993650. doi: 10.1038/s42005-021-00698-x. URL http://dx.doi.org/10.1038/s42005-021-00698-x.
12. G. Iadarola et al., Beam-induced heat loads on the LHC arc beam screens with different beam and machine configurations: experiments and comparison against simulations. Technical Report CERN-ACC-NOTE-2019-0057, CERN (Dec, 2019). URL https://cds.cern.ch/record/2705513.
13. G. Skripka and G. Iadarola, Beam-induced heat loads on the beam screens of the HL-LHC arcs. Technical Report CERN-ACC-NOTE-2019-0041, CERN (Oct, 2019). URL https://cds.cern.ch/record/2692753.
14. X. Buffat, S. Antipov, G. Arduini, R. De Maria, N. Karastathis, S. Kostoglou, A. Koval, E. H. Maclean, N. Mounet, Y. Papaphilippou, T. H. B. Persson, and R. Tomas Garcia, Strategy for Landau damping of head-tail instabilities at top energy in the HL-LHC. Technical Report CERN-ACC-NOTE-2020-0059, CERN (Nov, 2020). URL http://cds.cern.ch/record/2745703/files/CERN-ACC-NOTE-2020-0059.pdf.
15. S. Redaelli, S. Antipov, N. Biancacci, A. Bertarelli, R. Bruce, F. Carra, G. Gobbi, A. Lechner, A. Mereghetti, and E. Metral, Staged implementation of low-impedance collimation in IR7: plans for LS2. Technical Report CERN-ACC-NOTE-2019-0001, CERN (Jan, 2019). URL http://cds.cern.ch/record/2654779/files/CERN-ACC-NOTE-2019-0001.pdf.
16. E. H. Maclean, R. Tomás, F. S. Carlier, M. S. Camillocci, J. W. Dilly, J. Coello de Portugal, E. Fol, K. Fuchsberger, A. Garcia-Tabares Valdivieso, M. Giovannozzi, M. Hofer, L. Malina, T. H. B. Persson, P. K. Skowronski, and A. Wegscheider, New approach to LHC optics commissioning for the nonlinear era, *Phys. Rev. Accel. Beams.* **22**, 061004 (Jun, 2019). doi: 10.1103/PhysRevAccelBeams.22.061004. URL https://link.aps.org/doi/10.1103/PhysRevAccelBeams.22.061004.
17. L. R. Carver, X. Buffat, K. Li, E. Métral, and M. Schenk, Transverse beam instabilities in the presence of linear coupling in the large hadron collider, *Phys. Rev. Accel. Beams.* **21**, 044401 (Apr, 2018). doi: 10.1103/PhysRevAccelBeams.21.044401. URL https://link.aps.org/doi/10.1103/PhysRevAccelBeams.21.044401.

18. S. V. Furuseth and X. Buffat, Loss of transverse Landau damping by noise and wakefield driven diffusion, *Phys. Rev. Accel. Beams.* **23**, 114401 (Nov, 2020). doi: 10.1103/PhysRevAccelBeams.23.114401. URL `https://link.aps.org/doi/10.1103/PhysRevAccelBeams.23.114401`.
19. O. S. Brüning, P. Collier, P. Lebrun, S. Myers, R. Ostojic, J. Poole, and P. Proudlock, *LHC Design Report*. CERN Yellow Rep. Monogr., CERN, Geneva (2004). doi: 10.5170/CERN-2004-003-V-1.
20. S. Fartoukh, Achromatic telescopic squeezing scheme and application to the LHC and its luminosity upgrade, *Phys. Rev. ST Accel. Beams.* **16**, 111002 (2013).
21. S. Papadopoulou, F. Antoniou, T. Argyropoulos, M. Hostettler, Y. Papaphilippou, and G. Trad, Impact of non-Gaussian beam profiles in the performance of hadron colliders, *Phys. Rev. Accel. Beams.* **23**, 101004 (Oct, 2020). doi: 10.1103/PhysRevAccelBeams.23.101004. URL `https://link.aps.org/doi/10.1103/PhysRevAccelBeams.23.101004`.
22. R. Tomás, J. Keintzel, and S. Papadopoulou, Emittance growth from luminosity burn-off in future hadron colliders, *Phys. Rev. Accel. Beams.* **23**, 031002 (Mar, 2020). doi: 10.1103/PhysRevAccelBeams.23.031002. URL `https://link.aps.org/doi/10.1103/PhysRevAccelBeams.23.031002`.
23. P. Baudrenghien and T. Mastoridis, Transverse emittance growth due to rf noise in the high-luminosity lhc crab cavities, *Phys. Rev. ST Accel. Beams.* **18**, 101001 (Oct, 2015). doi: 10.1103/PhysRevSTAB.18.101001. URL `https://link.aps.org/doi/10.1103/PhysRevSTAB.18.101001`.
24. X. Buffat, W. Herr, T. Pieloni, and D. Valuch, Modeling of the emittance growth due to decoherence in collision at the Large Hadron Collider, *Phys. Rev. Accel. Beams.* **23**, 021002 (Feb, 2020). doi: 10.1103/PhysRevAccelBeams.23.021002. URL `https://link.aps.org/doi/10.1103/PhysRevAccelBeams.23.021002`.
25. S. Redaelli, R. Appleby, R. Bruce, O. Brüning, A. Kolehmainen, G. Ferlin, A. Foussat, M. Giovannozzi, P. Hermes, D. Mirarchi, D. Perini, A. Rossi, and G. Stancari, Hollow electron lenses for beam collimation at the high-luminosity large hadron collider (HL-LHC), *Journal of Instrumentation.* **16** (03), P03042 (Mar, 2021). doi: 10.1088/1748-0221/16/03/p03042. URL `https://doi.org/10.1088/1748-0221/16/03/p03042`.
26. D. Mirarchi, R. B. Appleby, R. Bruce, M. Giovannozzi, A. Mereghetti, S. Redaelli, and G. Stancari, Nonlinear dynamics of proton beams with hollow electron lens in the cern high-luminosity lhc, *The European Physical Journal Plus.* **137** (1), 7 (2021). doi: 10.1140/epjp/s13360-021-02201-5. URL `https://doi.org/10.1140/epjp/s13360-021-02201-5`.
27. S. Kostoglou, G. Arduini, Y. Papaphilippou, G. Sterbini, and L. Intelisano, Origin of the 50 Hz harmonics in the transverse beam spectrum of the large hadron collider, *Phys. Rev. Accel. Beams.* **24**, 034001 (Mar, 2021). doi: 10.1103/PhysRevAccelBeams.24.034001. URL `https://link.aps.org/doi/10.1103/PhysRevAccelBeams.24.034001`.
28. S. Kostoglou, G. Arduini, Y. Papaphilippou, G. Sterbini, and L. Intelisano, Impact of the 50 Hz harmonics on the beam evolution of the

large hadron collider, *Phys. Rev. Accel. Beams.* **24**, 034002 (Mar, 2021). doi: 10.1103/PhysRevAccelBeams.24.034002. URL `https://link.aps.org/doi/10.1103/PhysRevAccelBeams.24.034002`.

29. S. Kostoglou, H. Bartosik, Y. Papaphilippou, G. Sterbini, and N. Triantafyllou, Tune modulation effects for colliding beams in the High Luminosity Large Hadron Collider, *Phys. Rev. Accel. Beams.* **23**, 121001 (Dec, 2020). doi: 10.1103/PhysRevAccelBeams.23.121001. URL `https://link.aps.org/doi/10.1103/PhysRevAccelBeams.23.121001`.
30. S. Fartoukh and M. Giovannozzi, Dynamic aperture computation for the as-built CERN Large Hadron Collider and impact of main dipoles sorting, *Nucl. Instrum. Methods Phys. Res., A.* **671**, 10–23 (2011). doi: 10.1016/j.nima.2011.12.052.
31. M. Giovannozzi, A proposed scaling law for intensity evolution in hadron storage rings based on dynamic aperture variation with time, *Phys. Rev. ST Accel. Beams.* **15**, 024001 (2012). doi: 10.1103/PhysRevSTAB.15.024001.
32. M. Giovannozzi and F. Van der Veken, Description of the luminosity evolution for the CERN LHC including dynamic aperture effects. Part I: the model, *Nucl. Instrum. Methods Phys. Res.* **A905**, 171–179 (2018). doi: 10.1016/j.nima.2019.01.072. [Erratum: Nucl. Instrum. Methods Phys. Res. A927, 471(2019)].
33. M. Giovannozzi and F. F. Van der Veken, Description of the luminosity evolution for the CERN LHC including dynamic aperture effects. Part II: application to Run 1 data, *Nucl. Instrum. Methods Phys. Res.* **A908**, 1–9 (2018). doi: 10.1016/j.nima.2018.08.019.
34. E. H. Maclean, M. Giovannozzi, and R. B. Appleby, Innovative method to measure the extent of the stable phase-space region of proton synchrotrons, *Phys. Rev. Accel. Beams.* **22**, 034002 (Mar, 2019). doi: 10.1103/PhysRevAccelBeams.22.034002. URL `https://link.aps.org/doi/10.1103/PhysRevAccelBeams.22.034002`.
35. E. H. Maclean, R. Tomás, F. Schmidt, and T. H. B. Persson, Measurement of nonlinear observables in the Large Hadron Collider using kicked beams, *Phys. Rev. Spec. Top. Accel. Beams.* **17**, 081002. 19 p (2014). doi: 10.1103/PhysRevSTAB.17.081002. URL `https://cds.cern.ch/record/2135840`.
36. R. De Maria, J. Andersson, L. Field, M. Giovannozzi, P. Hermes, N. Hoimyr, G. Iadarola, S. Kostoglou, E. Maclean, E. McIntosh, A. Mereghetti, J. Molson, V. Berglyd Olsen, D. Pellegrini, T. Persson, M. Schwinzerl, S. Singh, K. Sjobak, and I. Zacharov, SixTrack project: Status, runtime environment, and new developments. p. TUPAF02. 7 p (2019). doi: 10.18429/JACoW-ICAP2018-TUPAF02. URL `https://cds.cern.ch/record/2697441`.
37. R. De Maria and G. Iadarola, Xsuite (2022). `https://xsuite.readthedocs.io`.
38. N. Nekhoroshev, An exponential estimate of the time of stability of nearly-integrable Hamiltonian systems, *Russ. Math. Surv.* **32**, 1 (1977).
39. A. Bazzani, S. Marmi, and G. Turchetti, Nekhoroshev estimate for isochronous non resonant symplectic maps, *Cel. Mech.* **47**, 333 (1990).

40. G. Turchetti, Nekhoroshev stability estimates for symplectic maps and physical applications. In *Proc. of the Winter School*, vol. 47, *Springer Proceedings in Physics*, p. 223, Les Houches, France ('89) (1990).
41. A. Bazzani, O. Mazzarisi, M. Giovannozzi, and E. Maclean, Diffusion in stochastically perturbed Hamiltonian systems with applications to the recent LHC dynamic aperture experiments. In eds. S. Chattopadhyay, M. Cornacchia, and S. Di Mitri, *Proceedings, 2017 Nonlinear Dynamics and Collective Effects (NOCE) workshop on Particle Beam Physics: Arcidosso, Italy, 19–22 September 2017*, pp. 70–85, WSP (2019).
42. A. Bazzani, M. Giovannozzi, and E. Maclean, Analysis of the non-linear beam dynamics at top energy for the CERN Large Hadron Collider by means of a diffusion model, *Eur. Phys. J. Plus.* **135** (1), 77 (2020). doi: 10.1140/epjp/s13360-020-00123-2.
43. A. Bazzani, M. Giovannozzi, and C. Montanari, Probing the diffusive behaviour of beam-halo dynamics in circular accelerators. *Eur. Phys. J. Plus* **137**, 1264 (2022). https://doi.org/10.1140/epjp/s13360-022-03478-w.
44. G. Valentino, R. Aßmann, R. Bruce, F. Burkart, V. Previtali, S. Redaelli, B. Salvachua, G. Stancari, and A. Valishev, Beam diffusion measurements using collimator scans in the LHC, *Phys. Rev. ST Accel. Beams.* **16**, 021003 (Feb, 2013). doi: 10.1103/PhysRevSTAB.16.021003. URL https://link.aps.org/doi/10.1103/PhysRevSTAB.16.021003.
45. A. Gorzawski, R. B. Appleby, M. Giovannozzi, A. Mereghetti, D. Mirarchi, S. Redaelli, B. Salvachua, G. Stancari, G. Valentino, and J. F. Wagner, Probing LHC halo dynamics using collimator loss rates at 6.5 TeV, *Phys. Rev. Accel. Beams.* **23**, 044802 (Apr, 2020). doi: 10.1103/PhysRevAccelBeams.23.044802. URL https://link.aps.org/doi/10.1103/PhysRevAccelBeams.23.044802.
46. A. Apollonio, M. Brugger, L. Rossi, R. Schmidt, B. Todd, D. Wollmann, and M. Zerlauth, Roadmap towards high accelerator availability for the CERN HL-LHC era, *Proceedings of IPAC15, Richmond, US* (2015). URL https://cds.cern.ch/record/2141848/files/tupty053.pdf.
47. J. Coupard, H. Damerau, A. Funken, R. Garoby, S. Gilardoni, B. Goddard, K. Hanke, D. Manglunki, M. Meddahi, G. Rumolo, R. Scrivens, and E. Chapochnikova, LHC Injectors Upgrade, Technical Design Report, Vol. II: Ions. Technical Report CERN-ACC-2016-0041, CERN, Geneva (Apr, 2016). URL https://cds.cern.ch/record/2153863.
48. A. Lechner, P. Bélanger, I. Efthymiopoulos, L. Grob, B. Lindstrom, R. Schmidt, and D. Wollmann, Dust-induced beam losses in the cryogenic arcs of the CERN Large Hadron Collider, *Phys. Rev. Accel. Beams.* **25**, 041001 (2022). doi: 10.1103/PhysRevAccelBeams.25.041001.
49. J. Jowett, G. Arduini, R. Assmann, P. Baudrenghien, C. Carli, M. Lamont, M. S. Camillocci, J. Uythoven, W. Venturini, and J. Wenninger, First run of the LHC as a heavy-ion collider, *Proceedings of IPAC11, San Sebastian, Spain.* p. 1837 (2011). URL http://accelconf.web.cern.ch/AccelConf/IPAC2011/papers/tupz016.pdf.

50. J.M. Jowett, Colliding heavy ions in the LHC, *Proceedings of the International Particle Accelerator Conference 2018, Vancouver, Canada*. p. 584 (2018). URL https://accelconf.web.cern.ch/ipac2018/papers/tuxgbd2.pdf.
51. J. Jowett, C. B. Castro, W. Bartmann, C. Bracco, R. Bruce, J. Dilly, S. Fartoukh, A. Garcia-Tabares, M. Hofer, M. Jebramcik, J. Keintzel, A. Lechner, E. Maclean, L. Malina, T. Medvedeva, D. Mirarchi, T. Persson, B. Petersen, S. Redaelli, M. Schaumann, M. Solfaroli, R. Tomas, J. Wenninger, J. Coello, E. Fol, N. Fuster-Martinez, E. Holzer, A. Mereghetti, B. Salvachua, C. Schwick, M. Spitznagel, H. Timko, A. Wegscheider, and D. Wollmann, The 2018 Heavy-Ion Run of the LHC, *Proceedings of the 10th International Particle Accelerator Conference (IPAC2019): Melbourne, Australia, May 19–24, 2019*. p. 2258 (2019). doi: https://doi.org/10.18429/JACoW-IPAC2019-WEYYPLM2.
52. B. Abelev et al., Upgrade of the ALICE experiment: Letter of intent, *Journal of Physics G: Nuclear and Particle Physics*. **41** (8), 087001 (Jul, 2014). doi: 10.1088/0954-3899/41/8/087001. URL https://doi.org/10.1088%2F0954-3899%2F41%2F8%2F087001.
53. Z. Citron et al., Future physics opportunities for high-density QCD at the LHC with heavy-ion and proton beams, *HL/HE-LHC Workshop: Workshop on the Physics of HL-LHC, and Perspectives at HE-LHC Geneva, Switzerland, June 18–20, 2018, CERN-LPCC-2018-07* (2018). URL https://cds.cern.ch/record/2650176?ln=en.
54. R. Bruce, T. Argyropoulos, H. Bartosik, R. D. Maria, N. Fuster-Martinez, M. Jebramcik, J. Jowett, N. Mounet, S. Redaelli, G. Rumolo, M. Schaumann, and H. Timko, HL-LHC operational scenario for Pb-Pb and p-Pb operation, *CERN-ACC-2020-0011* (2020). URL https://cds.cern.ch/record/2722753.
55. R. Bruce, M. Jebramcik, J. Jowett, T. Mertens, and M. Schaumann, Performance and luminosity models for heavy-ion operation at the CERN Large Hadron Collider, *Eur. Phys. J. Plus.* **136**, 745 (2021). doi: 10.1140/epjp/s13360-021-01685-5. URL https://doi.org/10.1140/epjp/s13360-021-01685-5.
56. S. R. Klein, Localized beampipe heating due to e- capture and nuclear excitation in heavy ion colliders, *Nucl. Inst. & Methods A*. **459**, 51 (2001).
57. R. Bruce, D. Bocian, S. Gilardoni, and J. M. Jowett, Beam losses from ultraperipheral nuclear collisions between Pb ions in the Large Hadron Collider and their alleviation, *Phys. Rev. ST Accel. Beams*. **12** (7), 071002 (Jul, 2009). doi: 10.1103/PhysRevSTAB.12.071002.
58. R. Bruce, J. M. Jowett, S. Gilardoni, A. Drees, W. Fischer, S. Tepikian, and S. R. Klein, Observations of beam losses due to bound-free pair production in a heavy-ion collider, *Phys. Rev. Letters*. **99** (14), 144801 (2007). doi: 10.1103/PhysRevLett.99.144801. URL https://link.aps.org/doi/10.1103/PhysRevLett.99.144801.
59. M. Schaumann, J. M. Jowett, C. Bahamonde Castro, R. Bruce, A. Lechner, and T. Mertens, Bound-free pair production from nuclear collisions and the

steady-state quench limit of the main dipole magnets of the CERN Large Hadron Collider, *Phys. Rev. Accel. Beams.* **23**, 121003 (Dec, 2020). doi: 10.1103/PhysRevAccelBeams.23.121003. URL `https://link.aps.org/doi/10.1103/PhysRevAccelBeams.23.121003`.

60. R.W. Assmann, Collimators and Beam Absorbers for Cleaning and Machine Protection, *Proceedings of the LHC Project Workshop - Chamonix XIV, Chamonix, France*. p. 261 (2005).
61. R.W. Assmann et al., The Final Collimation System for the LHC, *Proc. of the European Particle Accelerator Conference 2006, Edinburgh, Scotland*. p. 986 (2006).
62. R. Bruce, R. W. Assmann, V. Boccone, C. Bracco, M. Brugger, M. Cauchi, F. Cerutti, D. Deboy, A. Ferrari, L. Lari, A. Marsili, A. Mereghetti, D. Mirarchi, E. Quaranta, S. Redaelli, G. Robert-Demolaize, A. Rossi, B. Salvachua, E. Skordis, C. Tambasco, G. Valentino, T. Weiler, V. Vlachoudis, and D. Wollmann, Simulations and measurements of beam loss patterns at the CERN Large Hadron Collider, *Phys. Rev. ST Accel. Beams.* **17**, 081004 (Aug, 2014). doi: 10.1103/PhysRevSTAB.17.081004. URL `http://link.aps.org/doi/10.1103/PhysRevSTAB.17.081004`.
63. R. Bruce, R. W. Assmann, and S. Redaelli, Calculations of safe collimator settings and β^* at the CERN Large Hadron Collider, *Phys. Rev. ST Accel. Beams.* **18**, 061001 (Jun, 2015). doi: 10.1103/PhysRevSTAB.18.061001. URL `http://link.aps.org/doi/10.1103/PhysRevSTAB.18.061001`.
64. R. Bruce, C. Bracco, R. D. Maria, M. Giovannozzi, A. Mereghetti, D. Mirarchi, S. Redaelli, E. Quaranta, and B. Salvachua, Reaching record-low β^* at the CERN Large Hadron Collider using a novel scheme of collimator settings and optics, *Nucl. Instrum. Methods Phys. Res. A.* **848**, 19–30 (Jan, 2017). doi: http://dx.doi.org/10.1016/j.nima.2016.12.039. URL `http://www.sciencedirect.com/science/article/pii/S0168900216313092`.
65. P. Hermes, R. Bruce, J. Jowett, S. Redaelli, B. S. Ferrando, G. Valentino, and D. Wollmann, Measured and simulated heavy-ion beam loss patterns at the CERN Large Hadron Collider, *Nucl. Instrum. Methods Phys. Res. A.* **819**, 73–83 (Feb, 2016). doi: http://dx.doi.org/10.1016/j.nima.2016.02.050. URL `https://www.sciencedirect.com/science/article/pii/S0168900216002175?via%3Dihub`.
66. N. Fuster-Martínez, R. Bruce, F. Cerutti, R. De Maria, P. Hermes, A. Lechner, A. Mereghetti, J. Molson, S. Redaelli, E. Skordis, A. Abramov, and L. Nevay, Simulations of heavy-ion halo collimation at the CERN Large Hadron Collider: Benchmark with measurements and cleaning performance evaluation, *Phys. Rev. Accel. Beams.* **23**, 111002 (Nov, 2020). doi: 10.1103/PhysRevAccelBeams.23.111002. URL `https://link.aps.org/doi/10.1103/PhysRevAccelBeams.23.111002`.
67. V. Previtali, *Performance evaluation of a crystal-enhanced collimation system for the LHC*. PhD thesis, EPFL, Lausanne (2010). URL `https://cds.cern.ch/record/1302274`. Presented on 07 Oct 2010.
68. D. Mirarchi, *Crystal Collimation for LHC*. PhD thesis, Imperial College, London (Aug, 2015). URL `http://cds.cern.ch/record/2036210`.

69. M. D'Andrea, *Applications of Crystal Collimation to the CERN Large Hadron Collider (LHC) and its High Luminosity Upgrade Project (HL-LHC)*. PhD thesis, University of Padova (Feb, 2021). URL `http://cds.cern.ch/record/2758839`. Presented 23 Feb 2021.